buildings

MDPI

Article

Characterization of Existing Steel Racks via Dynamic Identification

Claudio Bernuzzi, Claudia Pellegrino and Marco Simoncelli *

Department of Architecture, Built Environment and Construction Engineering (ABC), Politecnico di Milano, 20133 Milano, Italy; claudio.bernuzzi@polimi.it (C.B.); claudia.pellegrino@gmail.com (C.P.)
* Correspondence: marco.simoncelli@polimi.it

Abstract: Steel storage racks are widely used in logistics for storing materials and goods. Rack design is carried out by adopting the so-called design-assisted-by-testing procedure. In particular, experimental analyses must be carried out by rack producers on the key structural components in order to adopt the design approach proposed for the more traditional carpentry frames. For existing racks, i.e., those in-service for decades, it is required to evaluate the load carrying capacity in accordance with the design provisions currently in use. The main problem in several cases should be the appraisal of the key component performance, owing to the impossibility to obtain specimens from in-service racks without reduction or interruption of the logistic flows. To overcome this problem, a quite innovative procedure for the identification of the structural unknowns of existing racks has been proposed in the paper. The method is based on in-situ modal identification tests combined with extensive numerical analyses. To develop the procedure, cheap measurement systems are required, and they could be immediately applied to existing racks. A real case study is discussed, showing the efficiency of the procedure in the evaluation of the effective elastic stiffness of beam-to-column joints and base plate connections, that are parameters which remarkably affect the rack performance. The structural unknowns have been determined based on four sets of modal tests (two configurations on the longitudinal direction and two in the transversal direction) plus 9079 iterative structural analyses. The results obtained were then directly compared with experimental component tests, showing differences lower than 9%.

Keywords: modal identification; finite element (FE) models; parametric numerical analysis; steel rack frames; joint stiffness; Modal Assurance Criterion (MAC)

Citation: Bernuzzi, C.; Pellegrino, C.; Simoncelli, M. Characterization of Existing Steel Racks via Dynamic Identification. *Buildings* **2021**, *11*, 603. https://doi.org/10.3390/buildings11120603

Academic Editor: Nerio Tullini

Received: 2 November 2021
Accepted: 29 November 2021
Published: 1 December 2021

1. Introduction

In the last decades, the most commonly used structures for logistics, i.e., steel storage racks, have become progressively more important, owing to the remarkable increment of web marketing activities. Furthermore, their relevant role in society has been recently amplified by the COVID-19 pandemic. The latest progress in this field contributed significantly to guarantee a constant supply of essential goods, despite lockdowns and numerous working issues in different sectors.

Racks are typically made of thin-walled steel members (TWCF), obtained from coils cold-rolled in continuum [1,2]. An example of a typical rack is sketched in Figure 1, which is obtained by a regular sequence of upright frames connected to each other by pairs of pallet beams carrying the stored units. Moreover, the presence of nonlinear partial strength semi-rigid connections, the regular perforation systems along the uprights, the extensive use of monosymmetric members, and both geometrical and mechanical imperfections do not allow for a design based on pure theoretical approaches [3]. For these reasons, the European rack design code EN15512 [4] recommends the so-called design-assisted-by-testing procedure [5], which combines theoretical approaches developed for more traditional steel carpentry frames with experimental data able to represent the response of joints and components. In particular, specific tests are required to evaluate:

- The effective properties of the structural elements. Uprights and beams are cold-formed thin-walled elements, whose shape (Figure 2) strictly depends on rack producers. The beams have a boxed cross-section shape usually defined by the need to guarantee adequate support to the pallet units. Uprights are generally mono-symmetric cross-section members characterized by a set of regular perforations along with their height. For this reason, the effective properties (effective second moment of area and net area) have to be always experimentally evaluated [3].
- Performance of beam-to-column connections. The beam-to column joints are realized by brackets welded to the beam ends and mechanically connected to the uprights via hooks and tab. These joints are characterized by a non-linear response, a quite low stiffness, and an unstable hysteretic behavior [6–8]. It can be noted that the shape of the hysteresis loops changes significantly in subsequent cycles, showing an important loss of stiffness after the first cycle. However, a non-negligible issue associated with these connections is the low value of the yielding moments if compared with the ones of the connected beams. Great values of rotations are achieved and, as a consequence, a satisfactory level of ductility characterizes the joints without brittle fracture;
- Performance of base-plate connections. Base-plate connections are generally realized by a formed steel plate, which is anchored to the industrial concrete floor and bolted to the upright bottom end [9]. Performance of base-plate has been intensively studied during the last years by many authors, showing the great importance of a proper design of these connections to the seismic response of racks [10,11]. In particular, the modern frontier of research on rack frames is devoted on the development of useful base systems able to dissipate seismic energy or to isolate the rack frame [12–15].

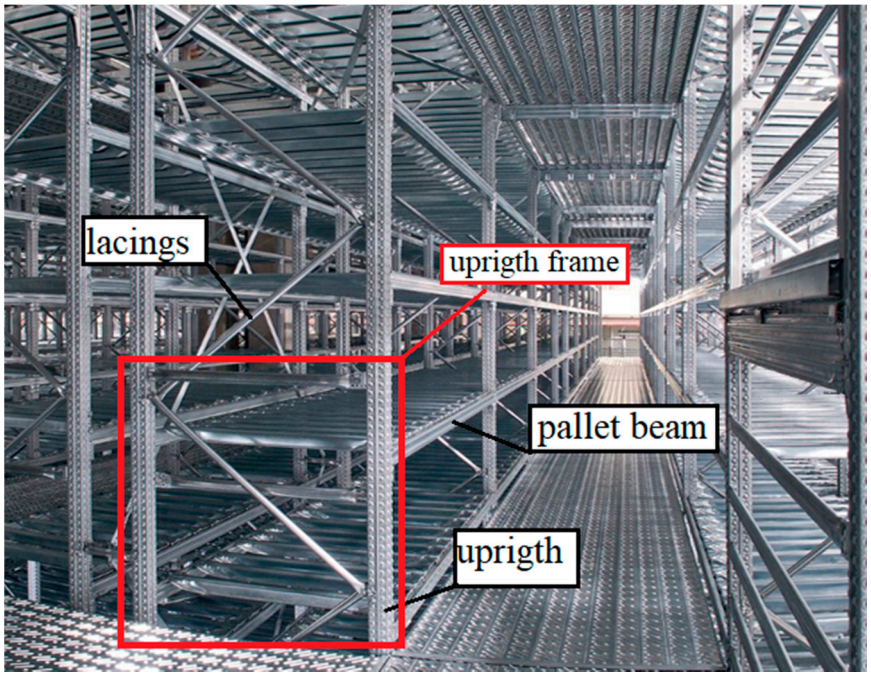

Figure 1. A typical steel rack with its main components.

Figure 2. Typical cross-sections: (**a**) uprights and (**b**) beams.

In addition, the shear deformability in the cross-aisle direction is an important parameter which influences the overall rack response. Upright frames are built-up trussed columns composed by lacings and vertical elements. Several tests and numerical models have been carried out showing that the shear stiffness of these elements cannot be directly appraised by using classic theoretical expressions [16]. Hence, ad-hoc strategies must be adopted, such as the reduction of the area of the bracings or the use of a suitably calibrated spring between bracing ends and the upright face.

Despite the regularity and simplicity of the structural rack schemes, a great number of research studies have recently addressed open problems in order to improve the efficiency of the design rules adopted for both static and seismic design. In particular, the most investigated aspects can be summarized in (i) warping influence on the member performance [17], (ii) assessment of the behavior (q) factor for the seismic design [18], (iii) post-earthquake effective performance [19], (iv) vulnerability assessment [20], and (v) fire protection [21].

Up to now, no attention has been paid to existing racks, i.e., to storage systems fully in-service and erected a few decades ago, for which it should be required to appraise the effective load carrying capacity in accordance with the current design provisions. For them, very limited structural data are generally available either because component tests were not executed at the time of erection or because the associated test reports are no longer available. These cases, whose occurrence increases over time, are extremely problematic because it is not possible to obtain specimens from the in-service structure to experimentally evaluate key structural data. As an alternative along with the rack substitution, innovative strategies based on non-destructive tests could hence be of paramount importance to allow for a structural design in accordance with the current provisions. Similar procedures were adopted in the past, for the identification of damages on steel frame and concrete structures [22–24].

The paper deals with the evaluation of the main structural characteristics of steel racks by means of in-situ non-destructive tests combined with parametric numerical analyses. The basic idea is to reproduce the experimental response of the structures via numerical finite element (FE) models. In particular, the dynamic rack identification (modal shapes and frequencies) is carried out via a set of accelerometers suitably located along the whole structures [25]. Then, the output of a great number of FE models differing for the values assumed by the unknown parameters must be processed till the best fit is achieved. For this reason, this characterization procedure can be usefully applied to cases of existing skeleton frames for which not all the design data are available.

A two-bay four-story rack has been considered for the applicative part and the elastic stiffnesses of both beam-to-column joints and base-plate connections have been assumed as unknown parameters, that have been determined based on four set of tests: two configurations on the longitudinal direction and two in the transversal direction. The same rack was already considered in the framework of a previous research [26], for which all component tests have been executed in accordance with EN15512 [4]. As a consequence, the direct comparison between the experimental and the numerically predicted values

allows for a concrete appraisal of the efficiency of the proposed procedure in predicting the unknown variables.

2. The Identification Procedure

For existing racks, all data related to the geometric layout, the weight of the pallet units as well as their location are usually available or can be easily evaluated in-situ. The proposed procedure can be applied through the following phases:

1. Geometric survey of the cross-section of the key components (uprights, pallets beams and diagonals) and identification of the unknown structural parameters, i.e., key components for which experimental or theoretical results are not available (e.g., the stiffness of beam-to-upright joints). The selection of the structural unknowns should be based on the experience and when the experience is low a preliminary sensitivity analysis is suggested;
2. Definition of the most efficient location of the accelerometers in the structure, execution of the in-situ tests and re-elaboration of the associated data in order to evaluate the experimental frequencies, the associated modal shapes and the structural damping;
3. Iterative numerical FE analyses. For each unknown parameter, a suitable range of variation has to be defined, and different values inside the ranges are considered. The number of unknown parameters defines the number of loops (Figure 3), and for each combination of the unknown parameters, a modal analysis is carried out recording the frequencies and the associate eigenvectors. Since the number of FE models associated with the values assumed by each unknown parameter should be very large, the above-described procedure could be suitably automatized by developing efficient interfaces able to run automatically the set of analyses and storing the output data of interest;
4. Comparison between the experimental and numerical data for each numerical case and appraisal of the accuracy of the model via the definition of a suitable accuracy parameter. The optimal solution (best match) is represented by the model characterized by the maximum accuracy and the associate values of the unknown parameters can be assumed as effective for practical design purposes.

The flowchart of the procedure is depicted in Figure 3 with reference to the case of two structural unknowns, identified as UK1 and UK2. For each of them, i.e., UKj, a set of values ranging from a minimum UKj_{min} and maximum UKj_{max} value, is considered with an increment of ΔUKj. The range of variability, i.e., the values assigned to UKj_{min} and UKj_{max} is strictly related to the sensibility of the operator. If the experience in this field is limited these values should range from 0 to a value close to ∞, with a great amount of time consuming. As an example, if the beam-to-column connections were considered, the EN1993-1-8 [27] boundary limits of semi-rigid connections could be used as a suitable range.

As far as phase 2 is concerned, the experimental data are organized as:

- Vector of experimental frequencies:

$$freq_{exp}(j) \tag{1}$$

where index $j \in \{1,2, \ldots M\}$ with M representing the number of modes experimentally found and of interest for the appraisal of the global response.

- Matrix of experimental modal displacements in the down-aisle (longitudinal or x) direction:

$$\phi_{x,exp}(n, j) \tag{2}$$

where index $n \in \{1, 2, \ldots N\}$ with N representing the number of nodes in which the modal displacements are extracted, that are the points in which the accelerometers are located.

- Matrix of experimental modal displacements in the cross-aisle (transversal or y) direction

$$\phi_{y,exp}(n,j) \tag{3}$$

At each iteration, i.e., for each FE model, the following quantities are stored:

- Values of the unknown parameters;
- Vector of the frequencies of the numerical modes:

$$freq_{num}(i) \tag{4}$$

where index $i \in \{1, 2, \dots P\}$ with P representing the number of numerical modes which satisfy the minimum threshold for the mass participating ratio, i.e., only the modes with a participating mass greater than 5% are considered.

- vector of the participating mass ratios of the numerical modes:

$$mass(i) = \max\{mass\_x(i),\ mass\_y(i)\} \tag{5}$$

where *mass_x(i)* and *mass_y(i)* are the participating mass ratios of the *i-th* mode along the x-direction and y-direction, respectively.

- matrix of numerical modal displacement in the longitudinal (x) direction:

$$\phi_{x,num}(n,i) \tag{6}$$

- matrix of numerical modal displacement in the transversal (y) direction:

$$\phi_{y,num}(n,i) \tag{7}$$

As to phase 4, it is worth noting that, the comparison between FE results and the experimental ones is carried for each combination of the unknown parameters out via three steps:

- Assessment of the MAC (Modal Assurance Criterion) matrix, in which the sole numerical modal shapes are correlated to the experimental ones, according to previous studies [28].
- Definition of a suitable accuracy matrix, in which also the differences between numerical and experimental frequencies are considered.
- Selection of the best match between the numerical and the experimental responses and evaluation of the associated accuracy.

In particular, according to the well-established MAC definition proposed in the literature, the correlation between two sets of modal vectors $\phi_{A,num}$ (numerical set) and $\phi_{A,exp}$ (experimental set) can be evaluated by computing a matrix (*MAC matrix*) as:

$$MAC(i,j) = \frac{\left|\{\phi_{A,num}\}_i^T \{\phi_{A,exp}\}_j\right|^2}{\left(\{\phi_{A,num}\}_i^T \{\phi_{A,num}\}_i\right)\left(\{\phi_{A,exp}\}_j^T \{\phi_{A,exp}\}_j\right)} \tag{8}$$

where $\{\phi_{A,num}\}_i$ is the column vector of the set $\phi_{A,num}$ related to the *i-th* mode and $\{\phi_{A,exp}\}_j$ is the column vector of the set $\phi_{A,exp}$ related to the *j-th* mode. Moreover, with superscript T is indicated the transposed vector.

The component $MAC(i,j)$ has the form of a coherency coefficient between the numerical mode i and the experimental j one and it ranges from 0 (no correlation) to 1 (numerical data fits perfectly the experimental ones). More in detail, a $MAC(i,j)$ value greater than 0.80 is in general considered a good match while a *MAC* value less than 0.40 is considered a poor match.

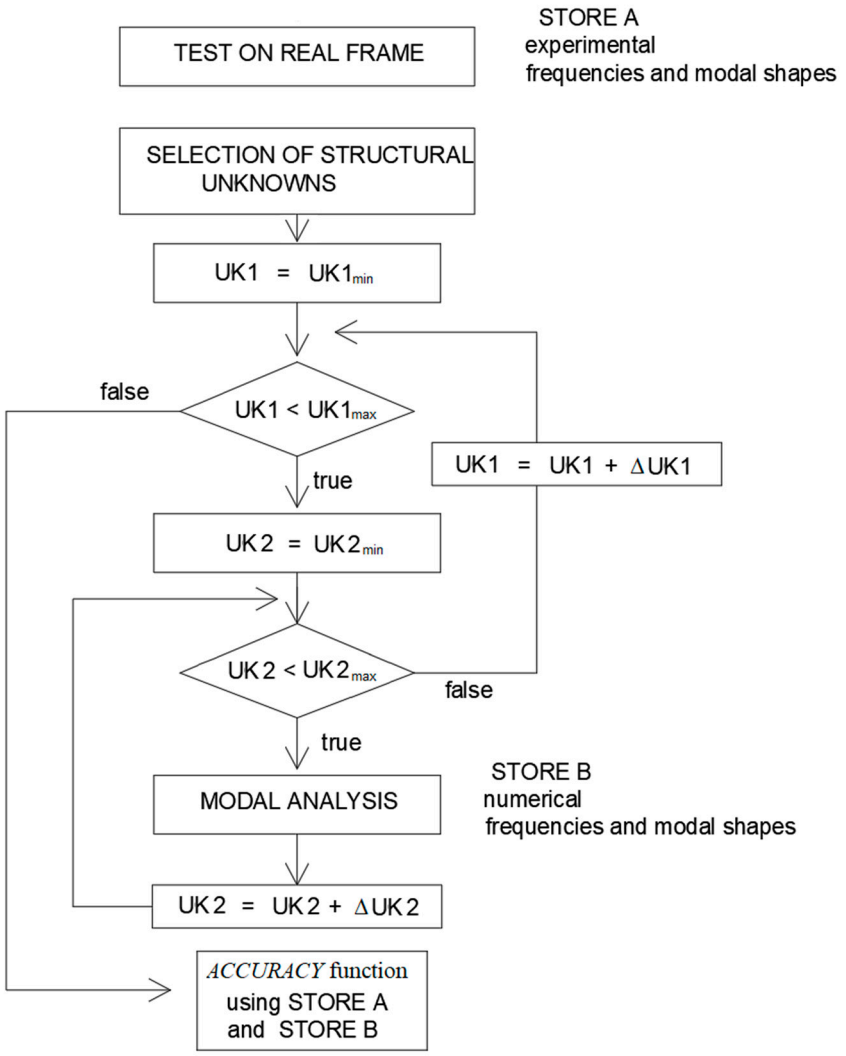

Figure 3. Flow chart of the proposed procedure.

Usually, the rack experimental modal shapes are uncoupled in the two main directions and for this reason, two independent *MAC* matrices must be evaluated, one referred to the down-aisle direction, mac_x, and the other to the cross-aisle direction, mac_y, defined as:

$$mac_x(i,j) = \frac{\left(\sum_{n=1}^{N} \phi_{x,num}(n,i) * \phi_{x,exp}(n,j)\right)^2}{\left(\sum_{n=1}^{N} \phi_{x,num}(n,i)\right)^2 * \left(\sum_{n=1}^{N} \phi_{x,exp}(n,j)\right)^2} \quad (9)$$

$$mac_y(i,j) = \frac{\left(\sum_{n=1}^{N} \phi_{y,num}(n,i) * \phi_{y,exp}(n,j)\right)^2}{\left(\sum_{n=1}^{N} \phi_{y,num}(n,i)\right)^2 * \left(\sum_{n=1}^{N} \phi_{y,exp}(n,j)\right)^2} \quad (10)$$

Then, a unified MAC matrix can be suitably defined as:

$$MAC(i,j) = \sqrt{(mac_x(i,j))^2 + (mac_y(i,j))^2} \quad (11)$$

It is worth to notice that in general the *MAC* matrix could be rectangular with the number of the numerical modes different from the experimental ones. Furthermore, the *MAC* definition is based only on the modal shapes and it does not seem sufficient to capture the effective accuracy of the numerical model, being ignored the contributions of the frequencies and the associated participating mass. To best fit experimental data,

an accuracy matrix $ACC(i,j)$ has been proposed in the framework of the present study, defined as:

$$ACC(i,j) = \left| \frac{\min\left(freq_{num}(i),\ freq_{exp}(j)\right)}{\max\left(freq_{num}(i),\ freq_{exp}(j)\right)} \right| * \frac{mass(i)}{mass_{tot}} * MAC(i,j) \tag{12}$$

where $mass_{tot}$ is the sum of the modal participating mass ratios, *mass(k)*, of the selected numerical modes:

$$mass_{tot} = \sum_{k=1}^{P} mass(k) \tag{13}$$

where k is the number of the selected numerical modes. The generic component $ACC(i,j)$ provides a complete description of the difference between numerical mode i and experimental mode j, in terms of both modal shapes and frequencies, weighted by the modal participating mass ratio of the numerical mode i with respect to all the modes. The closer this value is to 1, the more similar the numerical mode i is to the experimental mode j in terms of frequencies and modal shape.

Starting from Equation (12), the final and most challenging task for each FE model is to quantify its accuracy in predicting the experimental response. To this purpose, a suitable parameter, ACC_{final}, has been defined, which has to be independent by the order in which the numerical modes are detected, by means of the following expression:

$$ACC_{max}(i) = \max(ACC(i,j)) \text{ with } j \in \{1,\ 2, \ldots M\} \tag{14}$$

$$ACC_{final} = \sum_{i=1}^{P} ACC_{max}(i) \tag{15}$$

The final accuracy, ACC_{final} is hence the sum of the chosen accuracy coefficients of interest, not necessarily located on the principal diagonal. This assumption usually leads to a number of numerical modes higher than the number of the experimental ones.

Finally, it is worth noting that a bi-univocal correspondence is required. If the numerical mode m corresponds to the two experimental ones (h and k), only the mode with the highest accuracy coefficient is selected. As an example, if $ACC(h,m) > ACC(k,m)$, the numerical mode m has to be associated with the sole h experimental mode. Then, the evaluation of the accuracy of the experimental mode k is carried out by excluding $ACC(k,m)$, already considered.

3. The Case Study: Characterization of a 2-Bay 4-Story Steel Rack

The procedure has been applied to a particular typology of steel storage rack (named shelving rack), commonly used to store light products [26]. In order to prove its efficiency, the values of the unknown parameters obtained from the characterization have been directly compared with the results of an experimentally campaign according to EN15512 [4], carried out few years ago.

3.1. Rack Description

The shelving rack of interest is made by three bays and four storage levels (Figure 4). The storage beams are connected in the transversal direction with removable shelf elements which create the supporting plane for the merchandize but do not contribute to the structural stiffening of the skeleton frame. All the members are made of steel S355 and the applied load is uniformly distributed on the frame and equal to 1kN on each couple of pallet beams. Load has been simulated by means of masonry bricks.

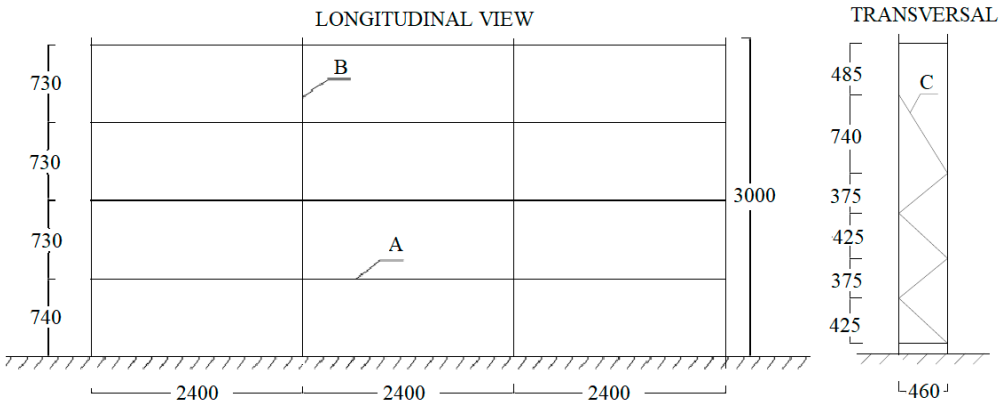

Figure 4. Scheme of the considered rack, dimensions in millimeters.

Uprights have a hollow T-like section with one axis of symmetry but, since the shear center and centroid are practically coincident, warping effects are hence negligible. The main cross-section characteristics are reported in Table 1 in terms of ratio between the gross area and its thickness (A/t), ratio between the second moment of area along the principal directions (I_y/I_z) and ratio between the shear center and the profile thickness (z_s/t). No direct data can be herein presented because components are commercial products. To account for the shear deformability of the upright frame, the area of diagonals has been reduced by a factor equal approximately to 0.3, recommended by the manufacturing engineer.

Table 1. Main properties of the considered sections.

	Pallet Beam (A)	**Upright (B)**	**Diagonal (C)**
	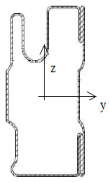	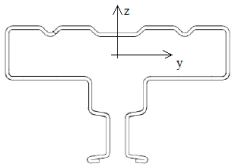	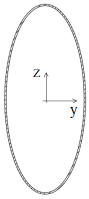
A/t	273	230	33
I_y/I_z	3.65	1.77	1.00
z_s/t	0.0	2.10	0.0

As previously mentioned, all data necessary for structural design are available for this rack. In particular, three nominally equal specimens of the beam-to-column joint were tested in cantilever configuration [4] and the associated experimental results are presented in Figure 5, in term of non-dimensional moment (moment of the connection, $M_{j,btc}$ divided by the yielding moment of the beam, M_b) versus rotation ϕ_{btc}. The mean value of the initial elastic stiffness ($S_{j,btc}$), which is represented by the thick dashed black line, assumes the experimental value of 1.17×10^7 Nmm/rad, which is the value of one unknown parameter to be assessed via the characterization procedure.

For baseplate connections, test results on three nominally equal specimens are available from the past research. The associated experimental curves are reported in Figure 6, in terms of relationships between the base-plate connection bending moment (M_{base}) divided by the resistant bending moment of the upright (M_c) versus rotation ϕ_{base}. Like for beam-to-column joints, initial elastic stiffness ($S_{j,base}$) is represented by a dashed thick black line, corresponding to the value of 2.21×10^6 Nmm/rad, which is the unknown stiffness to approximate via the characterization procedure.

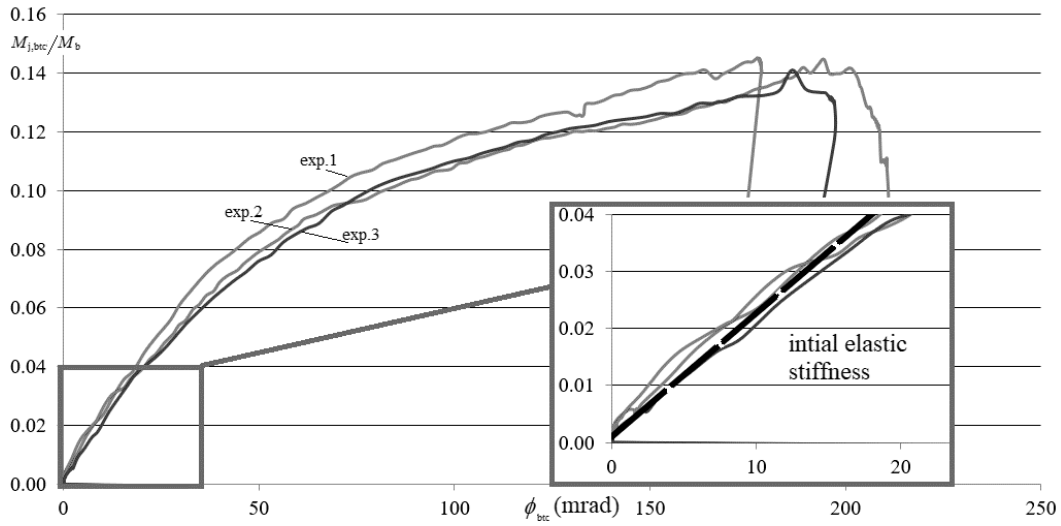

Figure 5. Relationship between the non-dimensional moment versus the rotation for beam-to-column joints and design value of the elastic stiffness.

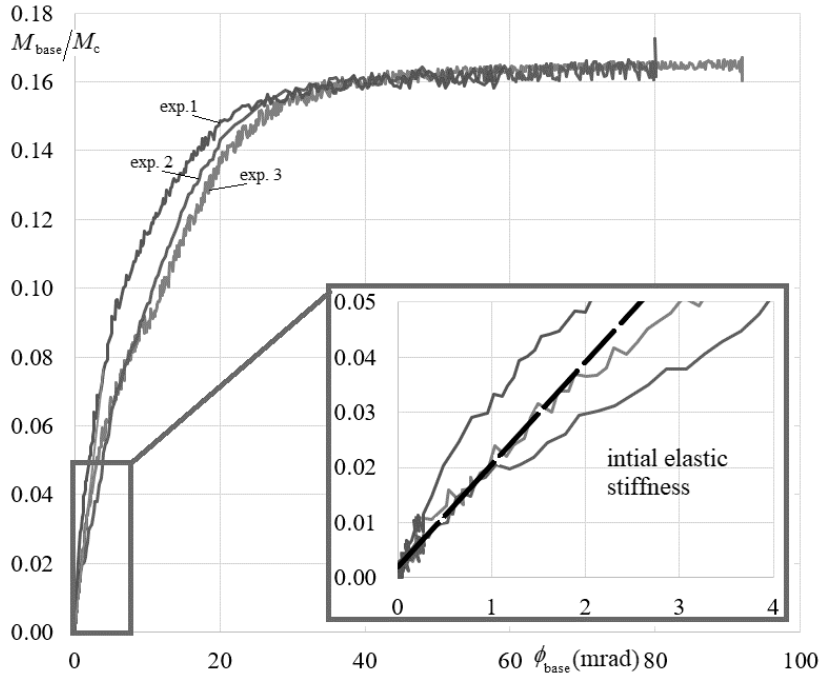

Figure 6. Relationship between the non-dimensional moment versus the rotation for base-plate connections and design value of the elastic stiffness.

3.2. In-Situ Modal Identification

Test setup (Figure 7) was comprised of PCB-393A03 mono-axial piezoelectric accelerometers with a sensitivity of 1000 mmV/g connected to IEPE (integrated electronic piezoelectric) National Instrument board. A constant excitation energy is given to the structure via an on-purpose built impact hammer, kinematically similar to a Charpy pendulum used to assess the steel toughness. Experimental tests were performed in both the down-aisle and the cross-aisle directions.

Two impact hammers were rigidly connected at the top of the rack in the longitudinal and transversal direction (Figure 7b). The height of falling and the excitation mass are 250 mm and 0.3 kg, respectively; therefore, the input energy was always constant during tests in order to guarantee that all test data are coherent to each other. The accelerations were recorded with a sampling frequency of 6400 Hz (Δt = 0.156 ms).

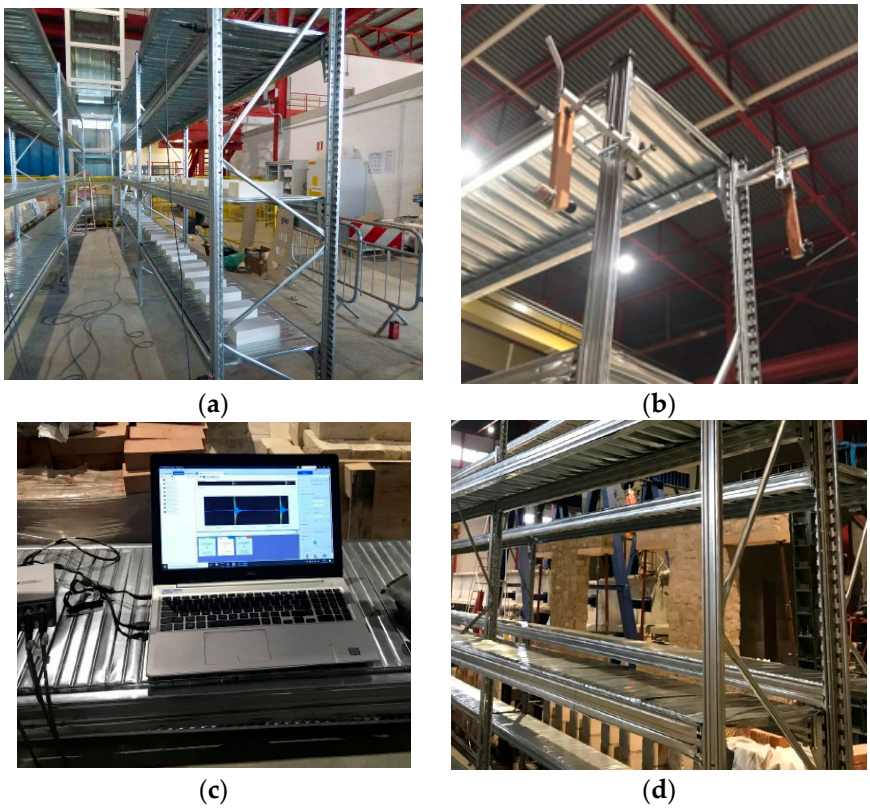

Figure 7. Experimental setup: (**a**) down-aisle view, (**b**) impact hammers, (**c**) data acquisition board, (**d**) cross-aisle view.

The final signal was elaborated by using the well-known Frequency Domain Decomposition (FDD) technique [29], paying attention to separate the predominant structural frequencies from external noise. In Figures 8 and 9 the obtained results in term of accelerations, frequencies, and deformed modal shapes are reported, which are related to the longitudinal and transversal direction, respectively. For the damping evaluation, reference has been made to the bandwidth method [29], which ensures a good estimation of the modal damping coefficient associated to each modal shape highlighted on the frequency domain.

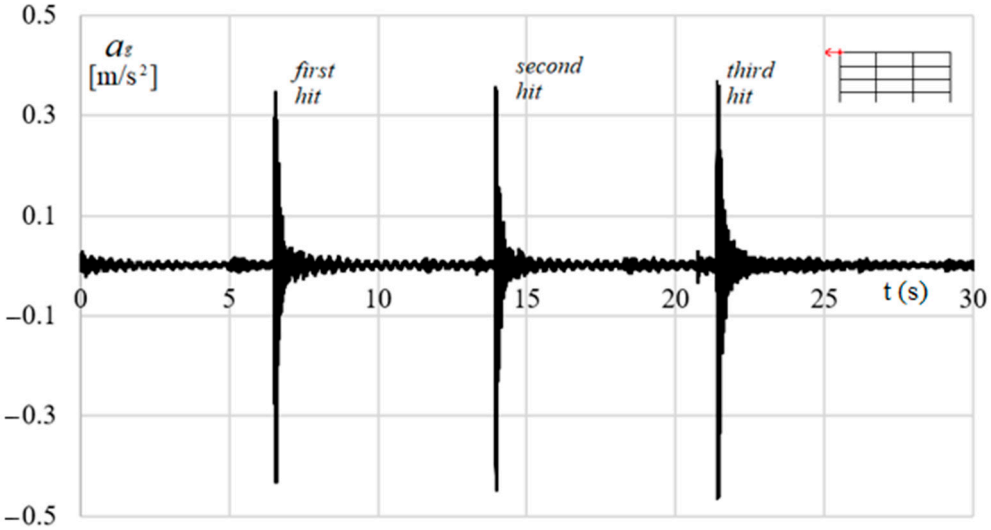

Figure 8. Example of an output obtained from the tests in longitudinal direction.

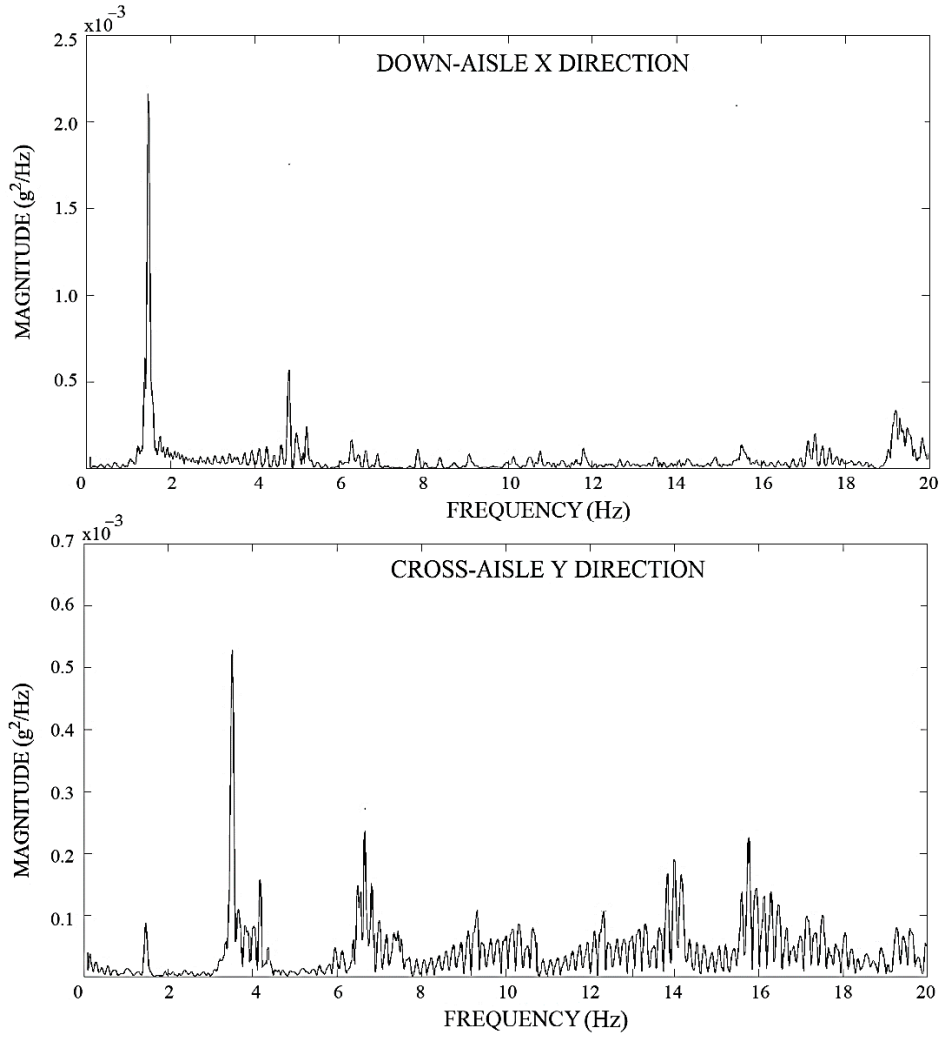

(**a**)

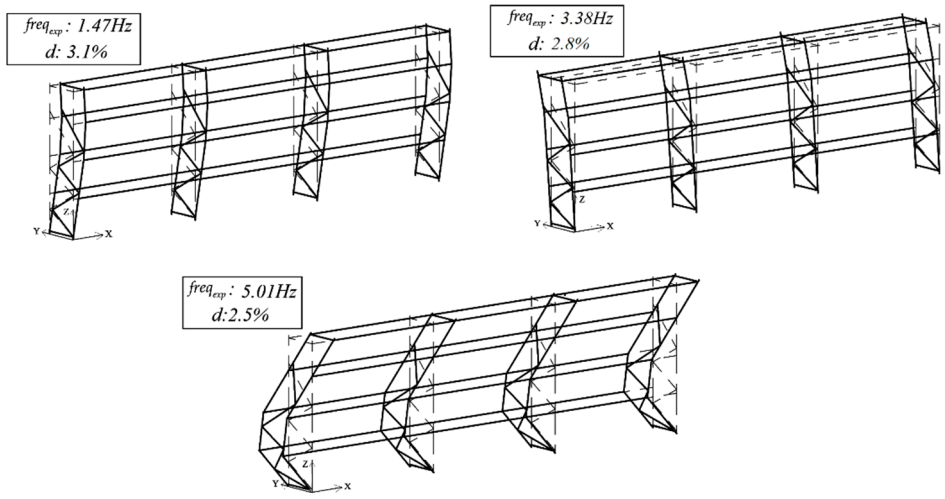

(**b**)

Figure 9. Key data related to the rack modal identification: (**a**) identified frequencies and (**b**) selected deformed shapes.

It can be noted that the highest magnitude is observed in the longitudinal direction, which is characterized by the predominant frequency (identified at 1.47 Hz) associated

with a pure flexural mode shape. This mode involves deformation of the points in the same direction with a maximum displacement located at the top storage level. The predominant frequency in transversal (cross-aisle) direction is in correspondence of 3.38 Hz and it is associated with a flexural mode. Other non-negligible magnitude can be observed at 5.01 Hz in longitudinal direction. In all the identified modes, the critical damping (d) is always lower than 5%, that is the default value recommended for steel structures.

3.3. Results

As previously mentioned, the elastic stiffness of both beam-to-column joints and base-plate connections have been considered as unknown parameters. Both these components have been modeled as link elements guaranteeing:

- Fixed translations along x, y, z axes;
- Fixed rotations about x and z axes;
- Linear moment-rotation curve about the y axis, whose slope is the unknown parameter (i.e., elastic stiffness).

The other rack components have been modeled by using the FE beam element.

As to the elastic stiffness of beam-to-column joints ($S_{j,btc}$), the range of variation was assumed between 0.9×10^7 and 1.2×10^7 Nmm/rad, with an increment of the trial values of 5×10^5 Nmm/rad. In total 7 different values have been considered for joints. For base-plate connections, the elastic stiffness ($S_{j,base}$) was assumed between 2×10^6 and 1×10^9 Nmm/rad with the increments of 1×10^4 Nmm/rad if the update stiffness is lower than 5×10^6 Nmm/rad, otherwise the increment was 1×10^6 Nmm/rad. In total 1297 different values have been considered for bases.

For both components, the ranges and the associated increments of the unknown parameters have been defined on the basis of the authors' expertise.

The time t_{TOT} required to best match the values of the unknown parameters can be appraised as:

$$t_{TOT} = N_{tot} * t \tag{16}$$

where t is the average time taken by the computer to perform one iteration (approximately 10 s) and N_{tot} is the number of the iterations (for the considered case $N_{tot} = 7 \times 1297 = 9079$). In total 25 h approximately have been required for the FE simulations associated with the present case studio. Final results are plotted in Figure 10, where for each trial combination, identified by a number ranging from 1 to 9079, the value of the associated accuracy parameter (ACC_{final}) is reported.

It can be that ACC_{final} ranges between 0.723 and 0.967 with sawtooth patterns, whose peaks are related to the extreme values of the unknown parameters during the different sets of iterations. Furthermore, part b) of the figure proposes a zoom related to the first 2200 cases, approximately, that is associated with the highest values of ACC_{final}. The combination n° 1852 is the best one, corresponding to $S_{j,btc} = 1.20 \times 10^7$ Nmm/rad and $S_{j,base} = 2.4 \times 10^6$ Nmm/rad with the highest value of ACC_{final} (=0.967). A direct comparison between these values and the experimental ones (Figures 5 and 6) shows that differences are lower than 9% and 8% with respect to beam-to-column joints and base-plate connections, respectively.

In both parts of the figure, some peaks are identified by a capital letter. For each of them, the number of the iteration, the corresponding values of the unknown parameters and the accuracy parameter are reported in Table 2. It is worth noting that ACC_{final} reaches in a great number of cases values significantly close to the unity, despite the fact that the corresponding elastic stiffnesses are remarkably different from those associated with case B. As an example, ACC_{final} is remarkably high for cases E and H, despite the fact that $S_{j,base}$ is more than two times more than the experimental one and/or the one associated with the best match.

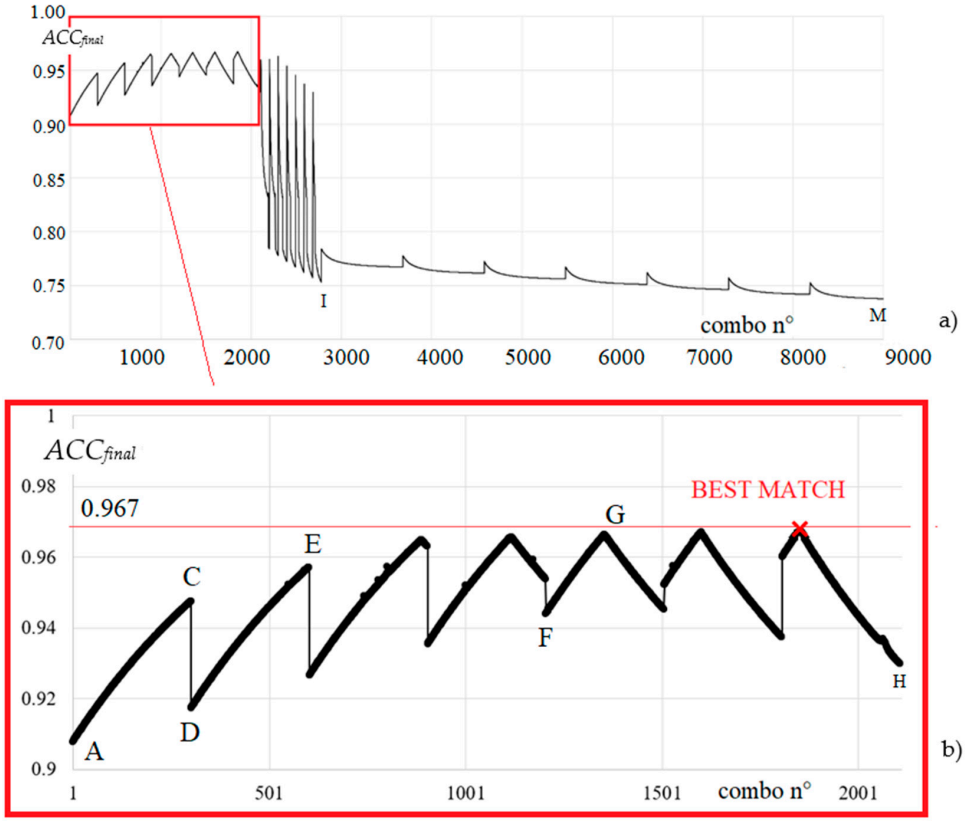

Figure 10. Accuracy: (**a**) total view and (**b**) zoom on the results closest to 1.

Table 2. Analysis results.

	Iteration	$S_{j,btc}$ (Nmm/rad)	$S_{j,base}$ (Nmm/rad)	ACC_{final}
A	1	0.90×10^7	2.0×10^6	0.905
C	301	0.90×10^7	5.0×10^6	0.951
D	302	0.95×10^7	2.0×10^6	0.911
E	602	0.95×10^7	5.0×10^6	0.957
F	1205	1.10×10^7	2.0×10^6	0.944
G	1350	1.10×10^7	3.5×10^6	0.965
B (*BEST MATCH*)	**1852**	$\mathbf{1.20 \times 10^7}$	$\mathbf{2.4 \times 10^6}$	**0.967**
H	2105	1.20×10^7	5.0×10^6	0.929
I	2870	1.00×10^7	9.7×10^8	0.767
M	9079	1.20×10^7	1.0×10^9	0.753

In order to appraise the influence of the elastic stiffness values on the rack performance, a reference can be made to Table 3. The values of the critical load multiplier (α_{cr}) associated with sole cases E, B, and H are reported, together with the ratio between the numerical frequency, $freq_{num}(i)$, over the experimental one $freq_{exp}(j)$, for the first two modes and the associated percentage (between brackets) of the participating mass. As to the evaluation of the critical load multiplier, α_{cr}, the one predicted by considering the effective value of the stiffnesses, i.e., the one deriving by the component tests, is 15.17, that is practically the value associated with the best match. Remarkable differences can be observed with references to the models E and H, i.e., 16.63 and 18.15, respectively. It is worth noting that α_{cr} is a parameter of paramount importance for the static as well as seismic design. A quite moderate overestimation of α_{cr}, like for E (9%) and H (19%) cases, should lead to an unsafe design. As to the prediction of the frequencies of the first two modes, i.e., the dominant

one, the errors associated with the best match are lower than 3% s, while for models E and H are up to 14%.

Table 3. Key design data related to models E, B and H.

	α_{cr}	$freq_{num}(1)/freq_{exp}(1)$ $(mass(1))$	$freq_{,num}(2)/freq_{exp}(2)$ $(mass(2))$
E (it. n. 602)	16.63	0.986 (88%)	1.053 (51%)
B (*BEST MATCH, it. n. 1852)*	15.21	0.999 (90%)	1.029 (52%)
H (it. n. 2105)	18.15	1.061 (88%)	1.029 (50%)

4. Conclusions

A refined procedure has been presented for the characterization of existing racks when it is not feasible to cut out details to perform direct laboratory tests to obtain key design parameters. In particular, rack behavior has to be clearly identified in terms of dynamic in-situ identification. The experimental response is then reproduced via numerical FE models differing for the values assigned to the unknown variables. The best fit in predicting experimental data is based on the definition of a suitable parameter, identified as ACC_{final}, depending on the well-known MAC matrix, by the frequencies and the associated modal masses (Equation (14b)). Despite in literature reference is made to the sole MAC index, the definition of ACC_{final} allows for a better characterization of the structure. In particular, making reference to the E, B, and H cases, it appears that the associated models are equivalent to each other, being MAC > 0.8, as it appears from Figure 11 by considering the red bold terms. It is hence not possible to understand which case better represents the structural behavior of the considered rack. Different conclusions derive from the use of the maximum ACC_{final} values, as discussed with reference to the critical load multiplier (Table 3).

MAC - E		numerical									
		1	2	3	4	5	6	7	8	9	10
experimental	1	**0.995**	0.525	0.787	0.396	0.015	0.051	0.005	0.030	0.185	0.017
	2	0.367	**0.991**	0.203	0.112	0.121	0.000	0.098	0.173	0.024	0.301
	3	0.019	0.020	0.237	0.016	0.581	0.526	**0.996**	0.957	0.127	0.019

MAC - B		numerical									
		1	2	3	4	5	6	7	8	9	10
experimental	1	**0.998**	0.530	0.792	0.410	0.036	0.050	0.082	0.170	0.014	0.009
	2	0.385	**0.991**	0.203	0.113	0.122	0.088	0.147	0.019	0.123	0.093
	3	0.011	0.021	0.232	0.009	0.035	0.048	0.368	0.021	0.147	**0.998**

MAC - H		numerical									
		1	2	3	4	5	6	7	8	9	10
experimental	1	**0.996**	0.530	0.793	0.414	0.041	0.049	0.094	0.187	0.016	0.001
	2	0.397	**0.991**	0.203	0.113	0.122	0.099	0.147	0.019	0.201	0.075
	3	0.016	0.021	0.231	0.009	0.016	0.048	0.312	0.011	0.032	**0.946**

Figure 11. Detail of the MAC matrices associated with different iteration.

Furthermore, it is worth noting that theoretically there is no limit to the number of unknows but, of course when these variables increase, the timing of the numerical process increase as well. Finally, it has to be remarked that field of applicability of the characterization procedure can be extended to all the types of structures for which the dynamic identification is required, independently of the structural typology or of the used material. Another application of the proposed procedure, once the structural characteristics of the frame have been determined, is the detection of the damages on the frames by using continuous monitoring systems [30].

Author Contributions: Conceptualization, C.B. and M.S.; analyses, C.P.; validation of results, C.B., C.P. and M.S.; draft preparation, C.B. and M.S.; writing—review and editing, C.B., C.P. and M.S.; supervision, M.S.; project administration, C.B. All authors have read and agreed to the published version of the manuscript.

Funding: This research received no external funding.

Institutional Review Board Statement: Not applicable.

Informed Consent Statement: Not applicable.

Data Availability Statement: For more data, contact the corresponding Authors.

Conflicts of Interest: The authors declare no conflict of interest.

Glossary

Latin symbols	
Small letters	
d	critical damping
$freq_{exp}(j)$	vector of experimental *j-th* frequency
$freq_{num}(i)$	vector of the frequency associated with the numerical *i-th* mode
mass(i)	vector of the participating mass ratios of the numerical *i-th* mode
$mass\_x\ (i)$	participating mass ratios of the *ith* mode in the x-direction
$mass\_y\ (i)$	participating mass ratios of the *ith* mode in the y-direction
$mac_x(i,j)$	Modal Assurance Criterion in the x-direction
$mac_y(i,j)$	Modal Assurance Criterion in the y-direction
$mass_{tot}$	sum of the modal participating mass ratios of all the numerical modes
t	average time taken by the computer to perform one iteration
z_s	distance between shear centre and centroid
Capitol letters	
A	cross-sectional area
$ACC(i,j)$	accuracy matrix
ACC_{final}	final accuracy value
E	Young Modulus of the beam
I_b	second moment of area of the beam
I_c	interstorey height of the upright
$I_{y/z}$	second moment of area in y/z direction
L_b	length of the beam
L_c	second moment of area of the upright
M	number of the experimental frequencies and modes
$MAC(i,j)$	Global Modal Assurance Criterion
M_b	bending resistance of the beam
M_c	bending resistance of the upright
$M_{j,base}$	bending resistance of the base connection
$M_{j,btc}$	bending resistance of the beam-to-column connection
N	nodal points in which modal displacements are known
N_{TOT}	number of iterations performed to find the final values of the selected unknowns
P	number of numerical frequencies and modal shapes
$S_{j,base}$	linear stiffness of the base-plate connection
$S_{j,btc}$	linear stiffness of the beam-to-column connection
t_{TOT}	time required to find the final values of the selected unknowns
UK_j	value of the structural unknown
$UK_{j,max}$	maximum value of the structural unknown
$UK_{j,min}$	minimum value of the structural unknown
Greek symbols	
α_{cr}	critical load multiplier
$\phi_{x,num}(n,i)$	matrix of numerical modal displacement in the longitudinal direction x
$\phi_{x,exp}(n,i)$	matrix of experimental modal displacements in the longitudinal direction
$\phi_{y,num}(n,i)$	matrix of numerical modal displacement in the transversal direction y
$\phi_{y,exp}(n,i)$	matrix of experimental modal displacements in the transversal direction
ϕ_{btc}	experimental beam-to-column joint rotation
ϕ_{base}	experimental base-plate connection rotation
ΔUK_j	step of the *j-* structural unknown
Δt	time step

References

1. Dubina, D.; Ungureanu, V.; Landolfo, R. Design of Cold-Formed Steel Structures. In *Eurocode 3: Design of Steel Structures—Part 1–3 Design of Cold-Formed Steel Structures, ECCS European Convention for Structural Steelworks*; Wilhelm Ernst & Sohn: Brussels, Belgium; Berlin, Germany, 2013.
2. Tilburgs, K. Those peculiar structures in cold-formed steel: 'racking and shelving'. *Steel Constr.* **2013**, *6*, 95–106. [CrossRef]
3. Baldassino, N.; Bernuzzi, C.; di Gioia, A.; Simoncelli, M. An experimental investigation on solid and perforated steel storage rack uprights. *J. Constr. Steel Res.* **2019**, *155*, 409–425. [CrossRef]
4. EN15512. *Steel Storage Systems—Adjustable Pallet Racking Systems—Principle for Structural Design*; European Committee for Standardization: Brussels, Belgium, 2021.
5. Baldassino, N.; Zandonini, R. Design by testing of industrial racks. *Adv. Steel Constr.* **2011**, *7*, 27–47. [CrossRef]
6. Dai, L.; Zhao, X.; Rasmussen, K.J.R. Cyclic performance of steel storage rack beam-to-upright bolted connections. *J. Constr. Steel Res.* **2018**, *148*, 24–48. [CrossRef]
7. Lyu, Z.J.; Wu, M.; Huang, Y.; Song, Y.; Cui, X. Assessment of the dynamic behavior of beam-to-column connections in steel pallet racks under cyclic load: Numerical investigation. *Adv. Civ. Eng.* **2018**, *2018*, 9243216. [CrossRef]
8. Bernuzzi, C.; Castiglioni, C.A. Experimental analysis on the cyclic behaviour of beam-to-column joints in steel storage pallet racks. *Thin-Walled Struct.* **2001**, *39*, 841–859. [CrossRef]
9. Petrone, F.; Higgins, P.; Bissonnette, N.; Kanvinde, A. The cross-aisle seismic performance of storage rack base connections. *J. Constr. Steel Res.* **2016**, *122*, 520–531. [CrossRef]
10. Maguire, J.R.; The, L.H.; Clifton, G.C.; Lim, J.P.B. Residual capacity of cold-formed steel rack uprights following stomping during rocking. *J. Constr. Steel Res.* **2019**, *159*, 189–197. [CrossRef]
11. Maguire, J.R.; The, L.H.; Clifton, G.C.; McCarthy, T.J. Equivalent static force method for selective storage racks with uplifting baseplates. *J. Constr. Steel Res.* **2020**, *165*, 105821. [CrossRef]
12. Maguire, J.R.; The, L.H.; Clifton, G.C.; Tang, Z.H.; Lim, J.P.B. Cross-aisle seismic performance of selective storage racks. *J. Constr. Steel Res.* **2020**, *168*, 105999. [CrossRef]
13. John, J.; Clifton, G.C.; Krishanu, R.; Lim, J.B.P. Three-storey modular steel building with a novel slider device: Shake table tests on a scaled down model and numerical investigation. *Thin-Walled Struct.* **2020**, *155*, 106932. [CrossRef]
14. John, J.; Clifton, G.C.; Krishanu, R.; Lim, J.B.P. Seismic protection of modular buildings with galvanised steel wall tracks and bonded rubber units: Experimental and numerical study. *Thin-Walled Struct.* **2021**, *162*, 107563. [CrossRef]
15. Simoncelli, M.; Tagliafierro, B.; Montuori, R. Recent development on the seismic devices for steel storage structures. *Thin-Walled Struct.* **2020**, *155*, 106827. [CrossRef]
16. Liu, S.; Pekoz, T.; Gao, W.L.; Ziemian, R.; Crews, J. Frame analysis and design of industrial rack structures with perforated cold-formed steel columns. *Thin-Walled Struct.* **2021**, *163*, 107755. [CrossRef]
17. Gabbianelli, G.; Kanyilmaz, A.; Bernuzzi, C.; Castiglioni, C.A. A combined experimental-numerical study on unbraced pallet rack under pushover. *Ing. Sismica* **2017**, *34*, 18–38.
18. Kanyilmaz, A.; Castiglioni, C.A.; Brambilla, G.; Chiarelli, G.P. Experimental assessment of the seismic behavior of unbraced steel storage pallet racks. *Thin-Walled Struct.* **2016**, *108*, 391–405. [CrossRef]
19. Bernuzzi, C.; Simoncelli, M. Seismic design of grana cheese cold-formed steel racks. *Buildings* **2020**, *10*, 246. [CrossRef]
20. Gabbianelli, G.; Cavalieri, F.; Nascimbene, R. Seismic vulnerability assessment of steel storage pallet racks. *Ing. Sismica* **2020**, *37*, 18–40.
21. Ren, C.; Zhang, P.; Yan, S.; Dai, L. Analysis and design of cold-formed steel rack uprights under localized fires. *Structures* **2020**, *27*, 2082–2095. [CrossRef]
22. Yu, L.; Chen, C. A hybrud ant lion optimizer with improved Nelder-Mead algorithm for structural damage detection by improving weighted trace lasso regularization. *Adv. Struct. Eng.* **2020**, *23*, 468–484. [CrossRef]
23. Chen, C.; Pan, C.; Chen, Z.; Yu, L. Structural damage detection via combinig weighted strategy with trace Lasso. *Adv. Struct. Eng.* **2019**, *22*, 597–612. [CrossRef]
24. Huang, M.; Zhao, W.; Gu, J.; Lei, Y. Damage identification of a steel frame based on integration of time series and neutral network under varying temperatures. *Hindawi-Adv. Civ. Eng.* **2020**, *2020*, 4284381. [CrossRef]
25. Gentile, C.; Gallino, N. Condition assessment and dynamic system identification of historic suspension footbridge. *Struct. Control Health Monit.* **2008**, *15*, 369–388. [CrossRef]
26. Bernuzzi, C.; di Gioia, A.; Gabbianelli, G.; Simoncelli, M. Pushover of Hand-loaded steel storage shelving racks. *J. Earthq. Eng.* **2017**, *21*, 1256–1282. [CrossRef]
27. CEN. *EN1993-1-8. Eurocode 3: Design of Steel Structures—Part 1–8: Design of Joints*; CEN: Brussels, Belgium, 2005.
28. Pastor, M.; Binda, M.; Harcarik, T. Modal Assurance Criterion. *Procedia Eng.* **2012**, *48*, 543–548. [CrossRef]
29. Brincker, R.; Zhang, L.; Andersen, P. Model identification of output only systems using Frequency Domain Decomposition. *Smart Mater. Struct.* **2001**, *10*, 441. [CrossRef]
30. Li, B.; Lei, Y.; Zhou, D.; Deng, Z.; Yang, Y.; Huang, M. Bearing Damage Detection of a Bridge under the Uncertain Conditions Based on the Bayesian Framework and Matrix Perturbation Method. *Shock Vib.* **2021**, *2021*, 5576362. [CrossRef]